



1 The characteristics of atmospheric brown carbon in Xi'an,  
2 inland China: sources, size distributions and optical properties

3  
4  
5  
6  
7  
8  
9  
10  
11  
12  
13  
14

Can Wu<sup>1,2</sup>, Gehui Wang<sup>1,2,3,4\*</sup>, Jin Li<sup>2</sup>, Jianjun Li<sup>2</sup>, Cong Cao<sup>2</sup>, Shuangshuang Ge<sup>1</sup>, Yuning Xie<sup>1</sup>, Jianmin Chen<sup>3,5</sup>, Xingru Li<sup>1,6</sup>, Guoyan Xue<sup>1</sup>, Xinpei Wang<sup>1</sup>, Zhuyu Zhao<sup>7</sup>, Fang Cao<sup>7</sup>

15 <sup>1</sup>Key Lab of Geographic Information Science of the Ministry of Education, School of  
16 Geographic Sciences, East China Normal University, Shanghai 210062, China

17 <sup>2</sup>Key Lab of Aerosol Physics and Chemistry, State Key Laboratory of Loess and Quaternary  
18 Geology, Institute of Earth Environment, Chinese Academy of Sciences, Xi'an 710061,  
19 China

20 <sup>3</sup>Institute of Eco-Chongming, 3663 North Zhongshan Road, Shanghai 200062, China

21 <sup>4</sup>CAS Center for Excellence in Regional Atmospheric Environment, Institute of Urban  
22 Environment, Chinese Academy of Sciences, Xiamen 361021, China

23 <sup>5</sup>Department of Environmental Science and Technology, Fudan University, Shanghai 200433,  
24 China

25 <sup>6</sup>Department of Chemistry, Analytical and Testing Center, Capital Normal University, Beijing  
26 100048, China

27 <sup>7</sup>Yale-NUIST Center on Atmospheric Environment, Nanjing University of Information  
28 Science & Technology, Nanjing 210044, China

29  
30  
31  
32  
33  
34

35 \*Corresponding author. Prof. Gehui Wang  
36 E-mail address: [ghwang@geo.ecnu.edu.cn](mailto:ghwang@geo.ecnu.edu.cn), or [wanggh@ieecas.cn](mailto:wanggh@ieecas.cn) (Gehui Wang)

37  
38  
39



40 **Abstract:** To investigate the characteristic of atmospheric brown carbon (BrC) in the  
41 semi-arid region of East Asia, PM<sub>2.5</sub> and size-resolved particles in the urban atmosphere of  
42 Xi'an, inland China during the winter and summer of 2017 were collected and analyzed for  
43 optical properties and chemical compositions. Methanol extracts (MeOH-extracts) were more  
44 light-absorbing than water extracts (H<sub>2</sub>O- extracts) in the optical wavelength of 300-600 nm,  
45 and well correlated with nitrophenols, polycyclic aromatic hydrocarbons (PAHs) and  
46 oxygenated PAHs ( $R^2 > 0.6$ ). The light absorptions ( $abs_{\lambda=365nm}$ ) of H<sub>2</sub>O- extracts and  
47 MeOH-extracts in winter were  $28 \pm 16$  M/m and  $49 \pm 32$  M/m, respectively, which are about 10  
48 times higher than those in summer, mainly due to the enhanced emissions from biomass  
49 burning for house heating. Water extracted BrC predominately occurred in the fine mode (<  
50 2.1  $\mu$ m) during winter and summer, accounting for 81% and 65% of the total absorption of  
51 BrC, respectively. The light absorption and stable carbon isotope composition measurements  
52 showed an increasing ratio of  $abs_{\lambda=365nm}$ -MeOH to  $abs_{\lambda=550nm}$ -EC along with an enrichment of  
53 <sup>13</sup>C in PM<sub>2.5</sub> during the haze development, indicating an accumulation of secondarily formed  
54 BrC (e.g., nitrophenols) in aerosol aging process. PMF analysis showed that biomass burning,  
55 fossil fuel combustion, secondary formation, and fugitive dust are the major sources of BrC in  
56 the city, accounting for 54.7%, 19%, 16.2%, and 10% of the total BrC of PM<sub>2.5</sub>, respectively.

57

58 **Key words:** Brown Carbon; Haze; Stable carbon isotope composition; Biomass burning;  
59 Secondary formation.

60

61



## 62 1. Introduction

63 Brown carbon (BrC) is a small fraction of carbonaceous aerosols, but it exhibits strong  
64 absorption abilities from near ultraviolet (UV) to visible light regions, and thus has been given  
65 extensive investigation in the recent decades (Laskin et al., 2015; Yan et al., 2018; Gustafsson  
66 et al., 2009). BrC has significant impact on climate change directly by absorbing solar  
67 radiation and indirectly by accelerating snowmelt and affecting the albedo (Qian et al.,  
68 2015; Andreae and Ramanathan, 2013). Based on the remote sensing observations and  
69 chemical transport models (Chung et al., 2012; Wang et al., 2014; Jo et al., 2016), a  
70 non-negligible positive radiative forcing by BrC was found on a global scale with a range  
71 from 0.1 to 0.6 W m<sup>-2</sup>. Beyond that, BrC also influence the atmospheric chemistry and human  
72 health. For example, BrC can shield polycyclic aromatic hydrocarbons (PAHs) from being  
73 oxidized, and thus substantially elevate lung cancer risk from PAHs (Hsu et al., 2014; Yan et  
74 al., 2018).

75 The sources of BrC are complicated, which can be primarily emitted from incomplete  
76 combustion of carbon-containing materials (e.g., biomass, coal and petroleum products.) and  
77 secondarily derived from aqueous-phase reaction (Sun et al., 2017; Gilardoni et al., 2016; Xie  
78 et al., 2018; Nakayama et al., 2013). Biomass burning was found to be a major primary source  
79 of BrC (Chen and Bond, 2010; Chakrabarty et al., 2010; Saleh et al., 2014), because lignin is of  
80 an unsaturated benzene-like structure, which is a chromophore group. Field measurements  
81 and laboratory studies found that BrC is also of secondary sources by forming chromophores  
82 during the atmosphere ageing process, e.g., high-NO<sub>x</sub> photooxidation (Liu et al., 2016; Xie et  
83 al., 2017), ozonolysis of aromatic precursors (Lee et al., 2014), and aqueous-phase



84 photochemical oxidation and polymerization (Smith et al., 2014; Flores et al., 2014; Bones et  
85 al., 2010). BrC products account for very small weight fraction of organic aerosol (OA), but  
86 have a significant effect on OA optical properties. For example, nitroaromatic compounds that  
87 are generated by photooxidation of toluene under high NO<sub>x</sub> conditions may account for  
88 40-60% of the total light absorption of toluene-SOA (Lin et al., 2015).

89 Multiple approaches have been developed to quantify the light absorption properties of  
90 BrC (Moosmuller et al., 2009), and a common and sensitive approach is the direct  
91 measurement of spectrophotometric properties of aerosol water or filter extracts by using  
92 optical instrumentation. The advantage of this method can avert interference from insoluble  
93 absorption material (e.g., black carbon) (Cheng et al., 2016; Shen et al., 2017), and supply  
94 high-resolution spectrum over a wide wavelength coverage. Furthermore, it is favorable for  
95 characterization of BrC light-absorbing components by combining with other analytical  
96 techniques, such as mass spectrometry (MS) (Laskin et al., 2015; Corr et al., 2012; Satish et al.,  
97 2017).

98 Xi'an is a metropolitan city located in Guanzhong Basin of inland China, which is a  
99 typical semiarid region in East Asia and have been suffering from serious particle pollution  
100 due to the large emission of anthropogenic pollutants (Wu et al., 2018; Wang et al., 2016; Wu  
101 et al., 2019), especially intensive coal combustion and biomass burning in winter for house  
102 heating (Wang et al., 2017). Many studies have been conducted on the BrC optical properties  
103 in China, but most of which were based on PM<sub>2.5</sub> and PM<sub>10</sub> sample collection and focused on  
104 the bulk aerosol optical properties with no information on the size distributions (Shen et al.,  
105 2017; Huang et al., 2018). In this study, both PM<sub>2.5</sub> and size-segregated aerosol samples in



106 Xi'an were collected during the 2017 winter and summer and analyzed for the characteristics  
107 of BrC. We firstly investigated the seasonal variations of chemical composition and  
108 light-absorption of BrC in the city, then discussed the size distribution of BrC and the impact  
109 of aerosol ageing process on BrC, and finally quantified its source contributions.

## 110 **2. Experimental section**

### 111 **2.1 Sample collection**

112 Aerosol samples with a 12-hr interval were collected using a high-volume ( $\sim 1.13 \text{ m}^3$   
113  $\text{min}^{-1}$ ) air sampler (Tisch Environmental, Inc., OH, USA) from December 31, 2016 to January  
114 22, 2017 (in winter) and from July 18 to August 6, 2017 (in summer). The sampler was  
115 installed on the roof of a three-story building on the campus of the Institute of Earth  
116 Environment, CAS (34.22°N, 108.88°E), which was located at the urban center of Xi'an,  
117 inland China. Meanwhile, size-resolved aerosols with 9 size bins (cutoff points were 0.43,  
118 0.65, 1.1, 2.1, 3.3, 4.7, 5.8, and 9.0  $\mu\text{m}$ , respectively) were collected by using an Anderson  
119 sampler at an airflow rate of 28.3  $\text{L min}^{-1}$  for 24 hr. All samples were collected onto the  
120 pre-baked (450°C for 6 hr) quartz filters and stored in a freezer (-18°C) prior to analysis.

### 121 **2.2 Chemical analysis**

122 A punch (0.526  $\text{cm}^3$ ) from each  $\text{PM}_{2.5}$  filter sample was analyzed for organic carbon (OC)  
123 and elemental carbon (EC) with a DRI Model 2001 Thermal/Optical Carbon Analyzer  
124 (Atmoslytic Inc., Calabasas, CA, USA) following the IMPROVE-A protocol (Chow et al.,  
125 2007). More details of the method including quality assurance and quality control (QA/QC)  
126 can be found elsewhere (Wang et al., 2010).

127 Partial filters were cut into pieces, and then extracted three times under sonication with



128 15ml Milli-Q pure water (18.2 MΩ). Ten ions such as  $\text{SO}_4^{2-}$ ,  $\text{NO}_3^-$ ,  $\text{Cl}^-$ ,  $\text{NH}_4^+$ , and  $\text{K}^+$  were  
129 determined using ion chromatography (Dionex, ICS-1100). Similar extraction processes were  
130 also applied to measure the water-soluble organic carbons (WSOC) of the samples by  
131 following the method of Wang et al. (2013). In order to analyze the organic compounds in the  
132 samples such as levoglucosan, PAHs, OPAH and nitrophenols, aliquot of the filter was  
133 extracted with a mixture of methanol and DCM (1:5, v/v), derivatized with BSTFA and  
134 measured by using gas chromatography (HP 7890A, Agilent Co., USA) coupled with mass  
135 spectroscopy detector (GC/MS) (HP 5975, Agilent Co., USA). Details of sample extraction  
136 and derivatization were documented elsewhere (Wang et al., 2009b; Ren et al., 2017). Stable  
137 carbon isotope composition of total carbon ( $\delta^{13}\text{C}_{\text{TC}}$ ) was determined by using an elemental  
138 analyzer (EA) (Carlo Erba, NA 1500) coupled with an isotope ratio mass spectrometer (IRMS,  
139 Finnigan MAT Delta Plus), more details of the method can be referred to elsewhere (Cao et al.,  
140 2016).

### 141 **2.3 Light absorption measurements**

142 Brown carbon (BrC) was extracted from a size of  $6\text{ cm}^3$  filter samples for 30min  
143 ultrasonication with 20ml Milli-Q pure water or methanol. All extracts were then filtered  
144 through  $0.45\text{ }\mu\text{m}$  PTFE (for water) and  $0.22\text{ }\mu\text{m}$  PES (for methanol) pore syringe filter to  
145 remove insoluble components and filter remnants. The light-absorption spectra were analyzed  
146 with a UV–visible spectrophotometer (AOE INSTRUMENTS, China) over a wavelength  
147 range of 190–900 nm (Hecobian et al., 2010). The absorption coefficient of water or methanol  
148 extracts ( $\text{M m}^{-1}$ ) could be calculated as the following equation (Teich et al., 2017):



149 
$$\text{abs}_\lambda = (A_\lambda - A_{700}) \frac{V_1}{V_a \times L} \times \ln(10) \quad (1)$$

150 Where  $A_\lambda$  and  $A_{700}$  were the light absorption of the extracts at the wavelength of  $\lambda$  and  
151 700nm, respectively.  $V_1$  represented the volume of the solvent extracting the filter sample, and  
152  $V_a$  was referred to the volume of air corresponding to the filter punch.  $L$  was the absorbing  
153 path length (i.e., 1 cm for the currently used quartz cuvettes). The  $\ln(10)$  was converted from  
154 base 10 (the form provided by the spectrophotometer) to natural logarithms. According to the  
155 previous studies, the absorption coefficient at 365nm was used as the brown carbon  
156 absorption in order to avoid disturbance of inorganic salts such as nitrate.

157 The bulk mass absorption coefficient (MAC,  $\text{m}^2/\text{g}$ ) of the extracts at a given wavelength  
158 can be described by the following equation:

159 
$$\text{MAC} = \frac{\text{abs}_\lambda}{C_{\text{W(OC)MSOC}}} \quad (2)$$

160 Where  $C_{\text{WS(OC)}}$  was the WSOC mass concentration of the water extracts or  
161 methanol-soluble organic carbon (MSOC) mass concentration of the methanol extracts. In this  
162 study, we assumed that OC could be completely dissolved in methanol solvent and substituted  
163 the MSOC to participate in the calculation. This hypothesis would lead to somewhat  
164 underestimation of the MAC of the methanol extracts, although high extraction efficiency of  
165 methanol solvent had reported by previous studies (Liu et al., 2013) .

166 The wavelength dependence of light-absorption with respect to the empirically defined  
167 power law relationship described by the following equation (Laskin et al., 2015):

168 
$$\text{MAC} = K\lambda^{-\text{AAE}} \quad (3)$$



169           Where  $K$  is a factor that includes aerosol mass concentrations, the AAE is termed as  
170 absorption Angström exponent. In this study, the AAE value of the filter extracts was  
171 determined by a linear regression of  $\log(\text{abs}_\lambda)$  versus  $\log(\lambda)$  over a wavelength range of  
172 300-450nm.

#### 173 **2.4 Positive Matrix Factorization (PMF) source apportionment**

174           PMF, as a receptor model, decomposes the sample matrix into two matrices (factor  
175 contributions and factor profiles), and has been widely used in source apportionment of  
176 atmospheric pollutants. More details on PMF can be found on the EPA website  
177 ([https://www.epa.gov/air-research/epa-positive-matrix-factorization-50-fundamentals-and-use-  
178 r-guide](https://www.epa.gov/air-research/epa-positive-matrix-factorization-50-fundamentals-and-use-r-guide)). In the present work, the mass concentrations of major species (OC, EC, WSOC,  
179  $\text{SO}_4^{2-}$ ,  $\text{NO}_3^-$ ,  $\text{NH}_4^+$ ,  $\text{Ca}^{2+}$ ), organic markers (benzo(b)fluoranthene (BbF), benzo(e)pyrene  
180 (BeP), indeno(1,2,3-c,d)pyrene (IP), levoglucosan, and nitrophenols), and  $\text{abs}_\lambda$  of water extracts  
181 have been used as the input data to perform the source apportionment for brown carbon with  
182 the EPA PMF 5.0 version, similar reports have been found elsewhere (Hecobian et al., 2010).  
183 The model was run numerous times with 3–7 factors and various combinations of the  
184 concentration and absorption data set. Base on the  $Q$  value ( $Q_{\text{true}}$  and  $Q_{\text{robust}}$ ) and  $r^2$ , which  
185 are indicative of the agreement of the model fit, four factors were obtained as the optimal  
186 solution.

### 187 **3. Results and discussion**

#### 188 **3.1 Carbonaceous species in $\text{PM}_{2.5}$ during summer and winter**

189           Figure 1 shows the temporal variations in the concentrations of  $\text{PM}_{2.5}$ , WSOC, OC and  
190  $\text{abs}_{\lambda=365\text{nm}}$  value during the two seasons. WSOC varied from 5.3 to 67  $\mu\text{g}/\text{m}^3$  in winter with an





191 average of  $23 \pm 13 \mu\text{g}/\text{m}^3$  (Table 1), which was 4.0 times higher than that in summer. OC  
192 exhibited a similar seasonal variation with WSOC with an average of  $41 \pm 25 \mu\text{g}/\text{m}^3$  in winter  
193 and  $8.4 \pm 2.4 \mu\text{g}/\text{m}^3$  in summer, respectively. Whereas, WSOC/OC ratio was much higher in  
194 summer ( $0.70 \pm 0.12$ ) than that in winter ( $0.58 \pm 0.13$ ), partly as a result of an enhanced  
195 photochemical formation of WSOC under the intense sunlight conditions, similar phenomena  
196 were also found in Beijing (Ping et al., 2017), Shanghai (Zhao et al., 2015a), Tokyo (Miyazaki  
197 et al., 2006) and Southeastern United States (Ding et al., 2008).

198 PAHs, OPAHs, and nitrophenols, as ubiquitous matters in the atmosphere, are mainly  
199 derived from combustion emission (e.g., coal, biomass) (Wang et al., 2015), although OPAHs  
200 and nitrophenols can also be derived from secondary formation (Lin et al., 2015; Xie et al.,  
201 2017). These matters are the efficient light-absorbing compounds due to owning specific  
202 light-absorbing molecular structures—BrC chromophores (Lin et al., 2017; Bluvshstein et al.,  
203 2017). Herein, 14 PAHs, 7 OPAHs, and 7 nitrophenols were examined for investigating their  
204 effect on BrC absorption. As seen in Figure S1, the temporal variations of PAHs, OPAHs, and  
205 nitrophenols were similar with levoglucosan, which is recognized as the tracer of biomass  
206 burning emissions, indicating that biomass burning is one of the major sources of these  
207 compounds. Concentrations of PAHs, OPAHs, and nitrophenols during winter were  $149 \pm 89$   
208  $\text{ng}/\text{m}^3$ ,  $174 \pm 98 \text{ ng}/\text{m}^3$  and  $17 \pm 12 \text{ ng}/\text{m}^3$  (Table 1), respectively, and were 10 - 43 times  
209 higher than those in summer, which can be explained by an increasing emission from  
210 residential heating during winter in the city and its surrounding regions.

211 As shown in Table S1,  $abs_{\lambda=365\text{nm}}$  extracted by methanol displays well correlations with  
212 PAHs, OPAHs, and nitrophenols, especially in winter ( $R^2 > 0.80$ ), which suggests that those



213 species are important light absorption contributors for BrC in Xi'an. Huang et al. (2018)  
214 found that PAHs and OPAHs in Xi'an accounted for, on average, 1.7% of the overall  
215 absorption of methanol-soluble BrC, but their mass fraction in OC was only 0.35%. A recent  
216 study reported that biomass burning also emitted nitroaromatic compounds, particularly  
217 nitrophenols, and accounted for 50-80% of the total visible light absorption ( $> 400$  nm) (Lin  
218 et al., 2017). The robust correlations of above compounds with the absorption at  $\lambda=365$  nm  
219 suggest that PAHs, OPAHs and nitrophenol are strong light-absorbing species.

## 220 **3.2 Light absorption of BrC in water and methanol extracts**

### 221 **3.2.1 Seasonal variations of light absorption by BrC**

222 As shown in Figure 2a and 2b, the marked feature of BrC in Xi'an is that the absorption  
223 spectrum increased notably from the visible to the ultraviolet ranges, and the average  
224  $\text{abs-MeOH}$  at  $\lambda=365$  nm was 1.5 - 1.7 times higher than  $\text{abs-H}_2\text{O}$  in the two seasons,  
225 indicating that MSOC provided a more comprehensive estimation for BrC. Due to enhanced  
226 emission of BrC, average  $\text{abs}_{\lambda=365\text{nm}}$  of BrC found in winter was  $49 \pm 32$  M/m for MeOH and  
227  $28 \pm 16$  M/m for WSOC, which were 9.5- and 8.1-fold higher than that in summer. This  
228 phenomenon was also observed in previous studies in Xi'an (Shen et al., 2017;Huang et al.,  
229 2018) and other areas of China (Du et al., 2014;Chen et al., 2018). Compared with other  
230 regions (Table 2), the absolute  $\text{abs}_{\lambda=365\text{nm}}$  values in Xi'an were slightly lower than that in  
231 Indo-Gangetic Plain, India (Satish et al., 2017;Bachi, 2016), but were considerably higher  
232 than that in Beijing, China (Du et al., 2014), US (Zhang et al., 2011) and Korea (Kim et al.,  
233 2016), suggesting that BrC pollution is more significant in Xi'an, a developing region in  
234 China. Furthermore, enhanced  $\text{abs}_{\lambda=365\text{nm}}$  loading in the nighttime was observed during the



235 two seasons, which can be ascribed to the shallower boundary layer height and the absence of  
236 photo-bleaching processes in nighttime (Saleh et al., 2013; Zhao et al., 2015b).

237 Linear regression slopes on the scatter plots of  $\text{abs}_{\lambda=365\text{nm}}$  values versus WSOC or OC  
238 represented the average of MAC at 365 nm (i.e.,  $\text{MAC}_{\text{WSOC}}$  and  $\text{MAC}_{\text{MSOC}}$ ). During winter,  
239 there was a slight disparity between the  $\text{MAC}_{\text{WSOC}}$  and  $\text{MAC}_{\text{MSOC}}$  with the averages of  $1.2 \pm$   
240  $0.06$  and  $1.3 \pm 0.03 \text{ m}^2/\text{g}$  (Figure 2e), respectively, which indicates that there are some similar  
241 chromophores of BrC between the two fractions.  $\text{abs}_{\lambda=365\text{nm}}$  showed a strong linear correlation  
242 with levoglucosan ( $R^2 > 0.97$ ), suggesting that abundant BrC may be largely derived from  
243 biomass burning. As shown in Fig. S2, mass ratios of levoglucosan/mannosan and  
244 levoglucosan/galacosan in the  $\text{PM}_{2.5}$  samples are similar to biomass types (i.e., woods, leaves,  
245 wheat straw), again reflecting that biomass burning combustion in Xi'an and its surrounding  
246 regions are probably the major sources of BrC in the city during winter. Compared to winter,  
247 the MAC in summer was slightly lower, which can be in part attributed to the less abundant  
248 light-absorbing PAHs and OPAHs due to no biomass burning for house heating. Moreover,  
249 with increasing photooxidation in summer, fragmentation reactions would occur and thus  
250 decrease light absorption for BrC aerosols, as reported by Sumlin et al. (2017), because higher  
251 levels of  $\text{O}_3$  and OH radicals in summer intensify the photooxidation and diminish the BrC  
252 aerosol light absorption by reducing the size of conjugated molecular systems. Interestingly,  
253 we found that the  $\text{MAC}_{\text{WSOC}}$  ( $1.1 \pm 0.2 \text{ m}^2/\text{g}$ ) in summer was significantly enhanced compared  
254 to  $\text{MAC}_{\text{MSOC}}$  ( $0.8 \pm 0.1 \text{ m}^2/\text{g}$ ), which can be ascribed to more amount of non-BrC in methanol  
255 extracts. The  $\text{abs}_{\lambda=365\text{nm}}$  showed a poor correlation with levoglucosan (Table S1), further  
256 indicating that the biomass burning was not the dominant source for BrC in summer.



257 Absorption Ångström exponents (AAE), which were derived from the filter methanol-  
258 and water-extracted BrC (AAE<sub>WSOC</sub> and AAE<sub>MSOC</sub>) for wavelengths between 300 and 450 nm,  
259 were  $6.1 \pm 9.7$  and  $5.3 \pm 8.5$  (Table 2) in winter, respectively, and resembled that in Beijing  
260 (Cheng et al., 2016), Guangzhou (Liu et al., 2018) and Indo- Gangetic Plain (Bachi, 2016),  
261 possibly indicating that the chemical compositions of BrC chromophores in these regions are  
262 similar during winter. As seen in Table 2, unlike those of H<sub>2</sub>O-extracts, the averaged values of  
263 MAC and AAE of MeOH extracts were 40% and 10% higher in winter than in summer,  
264 suggesting that chemical compositions of BrC are different between the two seasons in the  
265 city and the winter BrC contained more non-polar compounds that are of stronger  
266 light-absorbing ability.

### 267 3.2.2 Aerosol size distribution of BrC

268 Particles with different sizes are of different chemical compositions, and thus optical  
269 properties of BrC in different size of particles are also different (Zhang et al., 2015;Zhai et al.,  
270 2017). However, information on size distribution of BrC absorption is very limited. In this  
271 study, we mainly focused on the water-extracted samples, because particles deposited on the  
272 filter surface are unevenly distributed, making the quantifications of OC and EC in the  
273 size-segregated samples not accurate enough. As shown in Figure S3, there was a good  
274 relationship between the  $abs_{\lambda=365nm}$  ( $R^2 > 0.96$ ) of the samples collected by Anderson sampler  
275 and those collected by high-volume PM<sub>2.5</sub> sampler (Fig. S3), suggesting a good agreement  
276 between the two sampling methods.

277 As show in Figure 3,  $abs_{\lambda=365nm}$  presented a bimodal pattern during winter and summer,  
278 dominating at the fine mode ( $D_p < 2.1\mu m$ ) with relative contributions of 81% and 65% to the



279 total absorption in the two seasons, respectively. These proportions were similar to those  
280 reported for a forest wildfire event, which showed that 93% of the total BrC absorption was in  
281 the fine particles ( $0.10 < D_p < 1.0 \mu\text{m}$ ) (Lorenzo et al., 2018). Maximum absorptions were  
282 observed at 1.02 and  $0.71 \mu\text{m}$  ( $D_{pg}$ - geometric mean diameters, Figure 3a and 3b) in winter  
283 and summer, respectively, which is in agreement with the observations by Lei et al (2018),  
284 who found that the major peaks for BrC absorption were in the rang from  $0.5 \mu\text{m}$  to  $1.0 \mu\text{m}$  in  
285 urban and may shift toward smaller size ( $< 0.4 \mu\text{m}$ ) for particles released from burning  
286 experiments (Lei et al., 2018). However, the size distribution pattern of MAC was different  
287 from that of  $\text{abs}_{\lambda=365\text{nm}}$  in Xi'an, which presented a monomodal distribution with a peak in the  
288 fine mode ( $< 2.1 \mu\text{m}$ ) in winter and a bimodal distribution in summer with two peaks in the fine  
289 ( $< 2.1 \mu\text{m}$ ) and coarse ( $> 2.1 \mu\text{m}$ ) modes, respectively (Figure 3c and 3d). As seen in Figure 3c  
290 and 3d, the fine mode of MAC was around 50% larger in winter than that in summer,  
291 suggesting that water-soluble fraction of winter fine particles was more light-absorbing  
292 compared to that in summer, probably due to the summertime stronger bleaching effect.

### 293 **3.3 Underestimation of BrC absorption by solvent extraction methods**

294 A few studies pointed out that absorption properties of BrC extracted by bulk solution  
295 may not entirely reflect the light absorption by ambient aerosols. Here, we further calculated  
296 the light absorption of the samples using the Mie theory combined with an imaginary ( $k$ ,  
297 responsible for absorption) refractive index with assumptions that particles were spherical  
298 morphology and externally mixed with other light-absorbing components. The imaginary  
299 refractive index could be obtained from MAC using follow equation (Laskin et al., 2015):



$$k_{(\lambda)} = \frac{\rho \lambda \text{ abs}}{4\pi \times \text{WSOC}} = \frac{\rho \lambda \text{ MAC}}{4\pi} \quad (4)$$

300  
301 Where  $\rho$  ( $\text{g}/\text{cm}^3$ ) was particle density and assigned as 1.5, more details about Mie calculations  
302 can be referred to the study by Liu et al. (2013).

303 As noted above, most BrC aerosols were in the fine mode ( $<2.1\mu\text{m}$ ), thus, here we only  
304 focused on this fraction for the Mie calculations. The values of imaginary refractive in winter  
305 remains nearly constant (0.038-0.048) for different particle sizes at  $\lambda=365$  nm (Table 3),  
306 which was about two times smaller than that ( $0.093 \pm 0.049$ ) over Gangetic Plain, India  
307 (Shamjad et al., 2017). Values of  $k$  in summer were slight smaller when compared to those in  
308 winter, suggesting that the aerosols in summer were more aged. Sumlin et al. (2017) found  
309 that  $k$  decreases with the atmospheric aging from  $0.029 \pm 0.001$  to  $0.019 \pm 0.001$  at  $\lambda=375$  nm.  
310 However,  $k$  values in this study were 1.8 to 8.1 times higher than previously reported values  
311 from the United States (Liu et al., 2013; Washenfelder et al., 2015). This is because that  $\text{PM}_{2.5}$   
312 particles in Xi'an, China are enriched in BrC and the mass absorption coefficient was  
313 considerably higher than that in US. Figure 4 compares the difference between  $\text{abs}_{\lambda=365\text{nm}}$   
314 predicted by Mie theory and that extracted by the bulk solution. Mie theory predicted  
315  $\text{abs}_{\lambda=365\text{nm}}$  was 1.3-fold higher than that measured by the bulk solution, suggesting that the  
316 solvent extraction methods, which have commonly been used for atmospheric BrC  
317 measurements, could result in a significant underestimation on optical absorption of aerosols.

### 318 **3.4 The characteristic of BrC with the aerosol aging**

319 During the ageing process secondary organic aerosols (SOA) with strong chromophores  
320 can be generated and efficiently absorb solar radiation (Lin et al., 2014; Lin et al., 2016). From



321 Figure 5, it can be found that air quality in Xi'an during the winter varied from the clean  
322 ( $PM_{2.5} < 75 \mu\text{g}/\text{m}^3$ ) to the polluted conditions ( $PM_{2.5} > 75 \mu\text{g}/\text{m}^3$ ) from the period of 12<sup>th</sup>  
323 January to 19<sup>th</sup> January. Such a case provides an opportunity to investigate the changes in  
324 light-absorption by BrC during the aerosol ageing process.

325 As shown in Figure 5a and 5b,  $abs_{\lambda=365\text{nm}}$  extracted by water and MeOH in Xi'an during  
326 the campaign showed an increasing trend from 12<sup>th</sup> January to 19<sup>th</sup> January, which is similar  
327 to  $PM_{2.5}$  loadings but opposite to the visibility, indicating that BrC is one of the important  
328 factors leading to the visibility deterioration. From Figure 5b, it can also be seen that light  
329 absorption of water-extracts dominated over the total BrC absorption especially in daytime  
330 and showed a variation pattern similar to the  $PM_{2.5}$  (Figure 5a) and WSOC loadings (Figure  
331 5c), indicating a continuous formation of secondary BrC during the aerosol ageing process. To  
332 illustrate this point, the stable carbon isotopic composition ( $\delta^{13}\text{C}_{\text{TC}}$ ) of total carbon (TC) in the  
333 samples was measured. WSOC/OC showed a positive correlation with the  $\delta^{13}\text{C}_{\text{TC}}$ ,  
334 demonstrating an ageing process of aerosols during the haze development from 12<sup>th</sup> to 19<sup>th</sup>,  
335 January, although it was weak ( $r = 0.47$ ,  $n = 17$ ). Similar conclusions were also reported by  
336 Yang et al. (2004) and Pavuluri et al. (2015). From Figure 5c, increasing trends of OPAHs and  
337 nitrophenols were observed during the haze development, suggesting that more SOAs with  
338 chromophores were generated during such an aerosol ageing process, because these  
339 compounds are also of secondary origins. To exclude the possible impact of the changes in  
340 BrC source emissions, the values of PAHs/OC and levoglucosan/OC were applied in this study,  
341 because PAHs and levoglucosan emission factors are different for different  
342 sources (Nguyen-Duy and Chang, 2017). As shown in Fig. S4, both of values indistinctively



343 change during the aerosol ageing process, indicating that the increasing  $abs_{\lambda=365nm}$  are not  
344 caused by the changes in source emissions. Moreover, we found that  $MAC_{MSOC}$  values during  
345 the age process also increased (Figure 5a), further suggesting that the bleaching effect on  
346 light-absorbing BrC was reducing during the haze developing process.

347 EC, which is also called as black carbon, is one of the major absorbing aerosol  
348 components in the atmosphere (Collier et al., 2018; Peng et al., 2016). To further assess the  
349 relative contribution of BrC during the aerosol ageing process, we compared the mass  
350 absorption efficiency of EC at  $\lambda=550$  nm ( $7.5 \pm 1.2$  m<sup>2</sup>/g) with BrC by using the method  
351 reported from Yan et al. (2015) and Kirillova et al. (2014). As shown in Figure 5c, the  
352 concentrations of EC have a slight change in the haze period, so the changes in light  
353 absorption of EC remained nearly constant. However, the ratio of  
354  $abs_{\lambda=365nm}\text{-MeOH}/abs_{\lambda=550nm}\text{-EC}$  increasingly became larger along with the visibility  
355 deterioration from January 12<sup>th</sup> to January 19<sup>th</sup> (Fig. 5b), while the mass ratios of PAHs/EC,  
356 OPAHs/EC and nitrophenols /EC during the period showed a significant negative correlation  
357 with visibility (Fig. S5), further suggesting that the impact of BrC on the visibility was more  
358 significant in comparison with EC.

359 During the haze developing process organic aerosols are usually getting more aged and  
360 enriched in heavier <sup>13</sup>C due to the kinetic isotopic effect (KIE) (Wang et al., 2010). As shown  
361 in Figure 6a and b,  $\delta^{13}C$  of PM<sub>2.5</sub> samples presented a strong positive correlation with  $abs_{\lambda=365}$   
362  $nm\text{-MeOH}$  ( $R^2=0.68$ ) in the daytime, while there was no such a correlation in the nighttime  
363 during the haze period of January 12<sup>th</sup> -19<sup>th</sup>, indicating a daytime formation of secondary BrC.  
364 From Figure 6c and 6d, we also found that the correlation of  $abs_{\lambda=365\text{ nm}\text{-MeOH}}/ abs_{\lambda=550\text{ nm}\text{-EC}}$





365 ratio with nitrophenol was much stronger in daytime than in nighttime, which is opposite to  
366 the correlation of  $\text{abs}_{\lambda=365 \text{ nm}}\text{-MeOH} / \text{abs}_{\lambda=550 \text{ nm}}\text{-EC}$  ratio with PAHs. Nitrophenols can be  
367 produced from secondary photooxidation of phenol with  $\text{NO}_x$ , while PAHs are produced  
368 solely from direct emissions especially from coal and biomass burning for house heating. The  
369 opposite diurnal correlations of  $\text{abs}_{\lambda=365 \text{ nm}}\text{-MeOH} / \text{abs}_{\lambda=550 \text{ nm}}\text{-EC}$  ratio with nitrophenols and  
370 PAHs again revealed an enhanced formation of secondary BrC during the aerosol ageing  
371 process.

### 372 **3.5 Positive matrix factorization (PMF) analysis for BrC source apportionment**

373 In the current work, The EPA PMF 5.0 model was used for identifying the possible  
374 sources of BrC. Because the number of the collected samples in each season was not large  
375 enough, data from the two seasons were merged together to form a dataset of  $80 \times 12$  (80  
376 samples with 12 species) in order to obtain an accurate analysis according to the PMF user  
377 guide. The resolved source profiles (factors) represented the sources that influenced  
378 variability in the selected components throughout two seasons in Xi'an. Similar approach was  
379 also reported by Zhang et al. (2010). With several iterative testes, a solution with four factors  
380 was identified as the optimal solution. As shown in Table S2, the values of  $Q_{\text{true}}$  and  $Q_{\text{robust}}$   
381 were consistent, which indicates that the model fits the input data well. Furthermore, the  
382 correlation coefficient between input and model values ranged from 0.82 to 0.99 with an  
383 average 0.96, also implying that the model fit well. This assess method was widely used in  
384 previous studies (Ren et al., 2017; Wang et al., 2009a).

385 Figure7 shows the factor profiles resolved by the model. Factor 01 was characterized by  
386 high levels of BeF (52.4%), BeP (56.5%), and IP (67.2%), which were primarily derived from



387 coal combustion and vehicle exhausts (Kong et al., 2010;Ma et al., 2010;Harrison et al., 1996),  
388 further, relatively high OC (28.5%) and EC (25%) associated with this factor was well known  
389 tracers of exhaust emissions (Zong et al., 2016), so we identified Factor 01 as the source from  
390 fossil fuel combustion. Factor 02 (fugitive dust) shows high contribution of  $\text{Ca}^{2+}$  (66.8%) and  
391 a moderate loading of EC (39.3%). Ca, as one of the most abundant crustal elements, is  
392 largely from construction work, resuspended dust or soil sources (Chow et al., 2004;Han et al.,  
393 2007). In addition, EC was a well-known tracer of vehicular emissions (Dorado et al., 2003),  
394 so this factor can be attributed to the impact of vehicles passing with higher speeds, leading to  
395 resuspend non-tailpipe particles. Moreover, the concentrations of  $\text{Ca}^{2+}$  in the night were  
396 almost higher than that during the day time, with averages of  $1.8 \pm 1.56$  and  $1.43 \pm 0.85 \mu\text{g}/\text{m}^3$ ,  
397 respectively. This is consistent with time for transporting the construction wastes by lorry.  
398 Thus, factor 02 was identified as fugitive dust. Factor 03 was identified as secondary  
399 formation, as it is associated with high loadings of  $\text{NO}_3^-$  (62.8%),  $\text{SO}_4^{2-}$  (72.8%),  $\text{NH}_4^+$  (68.8%)  
400 and a moderate loading of OC and WSOC, indicating the presence of secondary inorganic and  
401 organic aerosols. The factor 04 showed high loadings with nitrophenols, levoglucosan, and  
402 abs-MeOH and was identified as biomass burning, because levoglucosan is the tracer for  
403 biomass burning smoke, and nitrophenols can be produced in the aging process of biomass  
404 burning plume.

405 Figure 8 shows the contributions of the above sources to the light absorption at  $\lambda=365\text{nm}$ ,  
406 which also represents the fraction of brown carbon for the factors. Biomass burning was the  
407 primary source of the BrC, accounting for 54.7% of the total BrC in the city, which is  
408 coincided with the results discussed in the section 3.2.1. A significant fraction (about 19%) of



409 BrC was associated with fossil fuel combustion. The fraction of secondary BrC was about  
410 16.2%, which was enhanced during the summer due to the efficient photochemical formation  
411 of secondary chromophores. The AAE value, closed to the aged SOA-AAE (4.7-5.3) (Bones  
412 et al., 2010), can also verify it. The remaining fraction of BrC was derived from the fugitive  
413 dust in the city. The results of BrC source apportionment for the Xi'an samples are in line  
414 with the work by Shen et al. (2017) and also similar to the results obtained in Beijing by using  
415 radiocarbon fingerprinting (Yan et al., 2017).

#### 416 **4. Conclusions**

417 This study investigated the seasonality of the light-absorption characteristics of BrC in  
418 Xi'an. Light absorption coefficient (MAC) of methanol-extracts at 365nm was 1.5-1.7 folds  
419 higher than that of water-extracts in the two seasons, suggesting non-polar compounds in the  
420 city are of stronger light-absorbing ability than that of polar compounds. The strong  
421 correlation of levoglucosan with BrC and the diagnostic ratios of levoglucosan/mannosan and  
422 levoglucosan/galacosan revealed that the wintertime abundant BrC ( $\text{abs}_{\lambda=365\text{nm}}\text{-MeOH}$  of  
423  $49.18 \pm 31.67 \text{ M/m}$ ) in Xi'an was mainly derived from the residential biofuel combustion for  
424 house heating in the city and its surrounding region. Size distribution results showed that 81%  
425 and 65% of BrC occurred in the fine mode ( $< 2.1\mu\text{m}$ ) during winter and summer, respectively,  
426 which is characterized by a monomodal size distribution with a peak in winter and a bimodal  
427 size distribution in summer with two peaks in the fine and coarse modes, respectively. The  
428 fine mode of MAC is 50% higher than that in summer, suggesting that the light-absorbing  
429 ability of wintertime fine particles is stronger, due to the abundant occurrence of PAHs and  
430 other aromatic compounds in the fine mode. The linear correlation between the ratio of



431  $\text{abs}_{\lambda=365\text{nm}}\text{-MeOHO}/\text{abs}_{\lambda=550\text{nm}}\text{-EC}$  and the enrichment of  $^{13}\text{C}$  during the haze development  
432 indicated an accumulation of secondary BrC in the aerosol ageing process. The daytime  
433 strong correlation of the ratio of  $\text{abs}_{\lambda=365\text{nm}}\text{-MeOHO}/\text{abs}_{\lambda=550\text{nm}}\text{-EC}$  with nitrophenols in the  
434 haze event further revealed that such an enhanced production of secondary BrC is related to  
435 the photooxidation of aromatic compounds with NO<sub>x</sub>. Source apportionment by using PMF  
436 showed that 55% of the BrC was associated with biomass burning in the city during the  
437 campaign, with 19 and 16% of BrC derived from fossil fuel combustion and secondary  
438 formation, respectively.

439  
440  
441

442 Author contributions. GW designed the experiment. CW, JiaL, JinL and CC collected the  
443 samples. CW and ZZ conducted the experiments. CW and GW performed the data  
444 interpretation and wrote the paper. All authors contributed to the paper with useful scientific  
445 discussions or comments.

446  
447  
448

449 Competing interests. The authors declare that they have no conflict of interest.

450  
451  
452

453 Acknowledgements. This work was financially supported by National Key R&D Plan  
454 (Quantitative Relationship and Regulation Principle between Regional Oxidation Capacity of  
455 Atmospheric and Air Quality (No. 2017YFC0210000), the program from National Nature  
456 Science Foundation of China (No. 41773117).

## 457 **References**

458 Andreae, M. O., and Ramanathan, V.: Climate change. Climate's dark forcings, *Science*, 340, 280-281,  
459 10.1126/science.1235731, 2013.



- 460 Bachi, S.: Mass absorption efficiency of light absorbing organic aerosols from source region of paddy-residue  
461 burning emissions in the Indo-Gangetic Plain, *Atmospheric Environment*, 125, 360-370,  
462 10.1016/j.atmosenv.2015.07.017, 2016.
- 463 Bluvshstein, N., Lin, P., Flores, J. M., Segev, L., Mazar, Y., Tas, E., Snider, G., Weagle, C., Brown, S. S., and  
464 Laskin, A.: Broadband optical properties of biomass burning aerosol and identification of brown carbon  
465 chromophores, *Journal of Geophysical Research*, 122, 10.1002/2016JD026230, 2017.
- 466 Bones, D. L., Henricksen, D. K., Mang, S. A., Gonsior, M., Bateman, A. P., Nguyen, T. B., Cooper, W. J., and  
467 Nizkorodov, S. A.: Appearance of strong absorbers and fluorophores in limonene-O<sub>3</sub>secondary organic  
468 aerosol due to NH<sub>4</sub><sup>+</sup>-mediated chemical aging over long time scales, *Journal of Geophysical Research*, 115,  
469 10.1029/2009jd012864, 2010.
- 470 Cao, F., Zhang, S.-C., Kawamura, K., and Zhang, Y.-L.: Inorganic markers, carbonaceous components and stable  
471 carbon isotope from biomass burning aerosols in Northeast China, *Science of the Total Environment*, 572,  
472 1244-1251, 10.1016/j.scitotenv.2015.09.099, 2016.
- 473 Chakrabarty, R. K., Moosmüller, H., Chen, L. W. A., and Lewis, K.: Brown carbon in tar balls from smoldering  
474 biomass combustion, *Atmospheric Chemistry and Physics*, 10, 6363-6370, 10.5194/acp-10-6363-2010,  
475 2010.
- 476 Chen, Y., and Bond, T. C.: Light absorption by organic carbon from wood combustion, *Atmospheric Chemistry  
477 & Physics Discussions*, 9, 1773-1787, 10.5194/acp-10-1773-2010, 2010.
- 478 Chen, Y., Ge, X., Chen, H., Xie, X., Chen, Y., Wang, J., Ye, Z., Bao, M., Zhang, Y., and Chen, M.: Seasonal light  
479 absorption properties of water-soluble brown carbon in atmospheric fine particles in Nanjing, China,  
480 *Atmospheric Environment*, 230-240, 10.1016/j.atmosenv.2018.06.002, 2018.
- 481 Cheng, Y., He, K. B., Du, Z. Y., Engling, G., Liu, J. M., Ma, Y. L., Zheng, M., and Weber, R. J.: The  
482 characteristics of brown carbon aerosol during winter in Beijing, *Atmospheric Environment*, 127, 355-364,  
483 10.1016/j.atmosenv.2015.12.035, 2016.
- 484 Chow, J. C., Watson, J. G., Kuhns, H., Etyemezian, V., Lowenthal, D. H., Crow, D., Kohl, S. D., Engelbrecht, J.  
485 P., and Green, M. C.: Source profiles for industrial, mobile, and area sources in the Big Bend Regional  
486 Aerosol Visibility and Observational study, *Chemosphere*, 54, 185-208,  
487 10.1016/j.chemosphere.2003.07.004, 2004.
- 488 Chow, J. C., Watson, J. G., Chen, L. W., Chang, M. C., Robinson, N. F., Trimble, D., and Kohl, S.: The  
489 IMPROVE\_A temperature protocol for thermal/optical carbon analysis: maintaining consistency with a  
490 long-term database, *Journal of the Air & Waste Management Association*, 57, 1014-1023,  
491 10.3155/1047-3289.57.9.1014, 2007.
- 492 Chung, C. E., Ramanathan, V., and Decremier, D.: Observationally-constrained Estimates of Carbonaceous  
493 Aerosol Radiative Forcing, *PROCEEDINGS OF THE NATIONAL ACADEMY OF SCIENCES OF THE  
494 UNITED STATES OF AMERICA*, 109, 11624-11629, 10.1073/pnas.1203707109, 2012.
- 495 Collier, S., Williams, L. R., Onasch, T. B., Cappa, C. D., Zhang, X., Russell, L. M., Chen, C.-L., Sanchez, K. J.,  
496 Worsnop, D. R., and Zhang, Q.: Influence of Emissions and Aqueous Processing on Particles Containing  
497 Black Carbon in a Polluted Urban Environment: Insights From a Soot Particle-Aerosol Mass Spectrometer,  
498 *Journal of Geophysical Research-Atmospheres*, 123, 6648-6666, 10.1002/2017jd027851, 2018.
- 499 Corr, C. A., Hall, S. R., Ullmann, K., and Anderson, B. E.: Spectral absorption of biomass burning aerosol  
500 determined from retrieved single scattering albedo during ARCTAS, *Atmospheric Chemistry and Physics*,  
501 12, 10505-10518, 10.5194/acp-12-10505-2012, 2012.
- 502 Ding, X., Zheng, M., Yu, L., Zhang, X., Weber, R. J., Yan, B., Russell, A. G., Edgerton, E. S., and Wang, X.:



- 503 Spatial and Seasonal Trends in Biogenic Secondary Organic Aerosol Tracers and Water-Soluble Organic  
504 Carbon in the Southeastern United States, *Environmental Science & Technology*, 42, 5171-5176,  
505 10.1021/es7032636, 2008.
- 506 Dorado, M. P., Ballesteros, E., Arnal, J. M., Gómez, J., and López, F. J.: Exhaust emissions from a Diesel engine  
507 fueled with transesterified waste olive oil ☆, *Fuel*, 82, 1311-1315, 10.1016/S0016-2361(03)00034-6, 2003.
- 508 Du, Z., He, K., Cheng, Y., Duan, F., Ma, Y., Liu, J., Zhang, X., Zheng, M., and Weber, R.: A yearlong study of  
509 water-soluble organic carbon in Beijing II: Light absorption properties, *Atmospheric Environment*, 89,  
510 235-241, 10.1016/j.atmosenv.2014.02.022, 2014.
- 511 Flores, J. M., Washenfelder, R. A., Adler, G., Lee, H. J., Segev, L., Laskin, J., Laskin, A., Nizkorodov, S. A.,  
512 Brown, S. S., and Rudich, Y.: Complex refractive indices in the near-ultraviolet spectral region of biogenic  
513 secondary organic aerosol aged with ammonia, *Physical Chemistry Chemical Physics*, 16, 10629-10642,  
514 10.1039/c4cp01009d, 2014.
- 515 Gilardoni, S., Massoli, P., Paglione, M., Giulianelli, L., Carbone, C., Rinaldi, M., Decesari, S., Sandrini, S.,  
516 Costabile, F., Gobbi, G. P., Pietrogrande, M. C., Visentin, M., Scotto, F., Fuzzi, S., and Facchini, M. C.:  
517 Direct observation of aqueous secondary organic aerosol from biomass-burning emissions, *Proceedings of  
518 the National Academy of Sciences of the United States of America*, 113, 10013-10018,  
519 10.1073/pnas.1602212113, 2016.
- 520 Gustafsson, O., Kruså, M., Zencak, Z., Sheesley, R. J., Granat, L., Engström, E., Praveen, P. S., Rao, P. S., Leck,  
521 C., and Rodhe, H.: Brown clouds over South Asia: biomass or fossil fuel combustion?, *Science*, 323,  
522 495-498, 10.1126/science.1164857, 2009.
- 523 Han, L., Zhuang, G., Cheng, S., Wang, Y., and Li, J.: Characteristics of re-suspended road dust and its impact on  
524 the atmospheric environment in Beijing, *Atmospheric Environment*, 41, 7485-7499,  
525 10.1016/j.atmosenv.2007.05.044, 2007.
- 526 Harrison, R. M., Smith, D. J. T., and Luhana, L.: Source Apportionment of Atmospheric Polycyclic Aromatic  
527 Hydrocarbons Collected from an Urban Location in Birmingham, U.K, *Environmental Science &  
528 Technology*, 30, 825-832, 10.1021/es950252d, 1996.
- 529 Hecobian, A., Zhang, X., Zheng, M., Frank, N., Edgerton, E. S., and Weber, R. J.: Water-Soluble Organic  
530 Aerosol material and the light-absorption characteristics of aqueous extracts measured over the  
531 Southeastern United States, *Atmospheric Chemistry and Physics*, 10, 5965-5977,  
532 10.5194/acp-10-5965-2010, 2010.
- 533 Hsu, H. I., Lin, M. Y., Chen, Y. C., Chen, W. Y., Yoon, C., Chen, M. R., and Tsai, P. J.: An integrated approach to  
534 assess exposure and health-risk from polycyclic aromatic hydrocarbons (PAHs) in a fastener manufacturing  
535 industry, *International Journal of Environmental Research & Public Health*, 11, 9578-9594,  
536 10.3390/ijerph110909578, 2014.
- 537 Huang, R. J., Yang, L., Cao, J., Chen, Y., Chen, Q., Li, Y., Duan, J., Zhu, C., Dai, W., and Wang, K.: Brown  
538 Carbon Aerosol in Urban Xi'an, Northwest China: The Composition and Light Absorption Properties,  
539 *Environmental Science & Technology*, 52, 6825-6833 10.1021/acs.est.8b02386, 2018.
- 540 Jo, D. S., Park, R. J., Lee, S., Kim, S. W., and Zhang, X. L.: A global simulation of brown carbon: implications  
541 for photochemistry and direct radiative effect, *Atmospheric Chemistry and Physics*, 16, 3413-3432,  
542 10.5194/acp-16-3413-2016, 2016.
- 543 Kim, H., Jin, Y. K., Jin, H. C., Ji, Y. L., and Lee, S. P.: Seasonal variations in the light-absorbing properties of  
544 water-soluble and insoluble organic aerosols in Seoul, Korea, *Atmospheric Environment*, 129, 234-242,  
545 10.1016/j.atmosenv.2016.01.042, 2016.



- 546 Kirillova, E. N., Andersson, A., Tiwari, S., Srivastava, A. K., Bisht, D. S., and Örjan, G.: Water-soluble organic  
547 carbon aerosols during a full New Delhi winter: Isotope-based source apportionment and optical properties,  
548 *Journal of Geophysical Research Atmospheres*, 119, 3476-3485, 10.1002/2013JD020041, 2014.
- 549 Kong, S., Ding, X., Bai, Z., Han, B., Chen, L., Shi, J., and Li, Z.: A seasonal study of polycyclic aromatic  
550 hydrocarbons in PM(2.5) and PM(2.5-10) in five typical cities of Liaoning Province, China, *J Hazard Mater*,  
551 183, 70-80, 10.1016/j.jhazmat.2010.06.107, 2010.
- 552 Laskin, A., Laskin, J., and Nizkorodov, S. A.: Chemistry of atmospheric brown carbon, *Chem Rev*, 115,  
553 4335-4382, 10.1021/cr5006167, 2015.
- 554 Lee, H. J., Aiona, P. K., Laskin, A., Laskin, J., and Nizkorodov, S. A.: Effect of solar radiation on the optical  
555 properties and molecular composition of laboratory proxies of atmospheric brown carbon, *Environmental  
556 Science & Technology*, 48, 10217-10226, 10.1021/es502515r, 2014.
- 557 Lei, Y., Shen, Z., Zhang, T., Zhang, Q., Wang, Q., Sun, J., Gong, X., Cao, J., Xu, H., and Liu, S.: Optical source  
558 profiles of brown carbon in size-resolved particulate matter from typical domestic biofuel burning over  
559 Guanzhong Plain, China, *Science of the Total Environment*, 622, 244-251, 10.1016/j.scitotenv.2017.11.353,  
560 2018.
- 561 Lin, G., Penner, J. E., Flanner, M. G., Sillman, S., Xu, L., and Zhou, C.: Radiative forcing of organic aerosol in  
562 the atmosphere and on snow: Effects of SOA and brown carbon, *Journal of Geophysical Research:  
563 Atmospheres*, 119, 7453-7476, 10.1002/2013jd021186, 2014.
- 564 Lin, P., Liu, J., Shilling, J. E., Kathmann, S. M., Laskin, J., and Laskin, A.: Molecular characterization of brown  
565 carbon (BrC) chromophores in secondary organic aerosol generated from photo-oxidation of toluene, *Phys  
566 Chem Chem Phys*, 17, 23312-23325, 10.1039/c5cp02563j, 2015.
- 567 Lin, P., Aiona, P. K., Li, Y., Shiraiwa, M., Laskin, J., Nizkorodov, S. A., and Laskin, A.: Molecular  
568 Characterization of Brown Carbon in Biomass Burning Aerosol Particles, *Environmental Science &  
569 Technology*, 50, 11815-11824, 10.1021/acs.est.6b03024, 2016.
- 570 Lin, P., Bluvshstein, N., Rudich, Y., Nizkorodov, S. A., Laskin, J., and Laskin, A.: Molecular Chemistry of  
571 Atmospheric Brown Carbon Inferred from a Nationwide Biomass Burning Event, *Environmental Science &  
572 Technology*, 51, 11561-11570, 10.1021/acs.est.7b02276, 2017.
- 573 Liu, J., Bergin, M., Guo, H., King, L., Kotra, N., Edgerton, E., and Weber, R. J.: Size-resolved measurements of  
574 brown carbon in water and methanol extracts and estimates of their contribution to ambient fine-particle  
575 light absorption, *Atmospheric Chemistry and Physics*, 13, 12389-12404, 10.5194/acp-13-12389-2013, 2013.
- 576 Liu, J., Lin, P., Laskin, A., Laskin, J., Kathmann, S. M., Wise, M., Caylor, R., Imholt, F., Selimovic, V., and  
577 Shilling, J. E.: Optical properties and aging of light-absorbing secondary organic aerosol, *Atmospheric  
578 Chemistry & Physics*, 16, 1-36, 2016.
- 579 Liu, J., Mo, Y., Ding, P., Li, J., Shen, C., and Zhang, G.: Dual carbon isotopes ( $^{14}\text{C}$  and  $^{13}\text{C}$ ) and optical  
580 properties of WSOC and HULIS-C during winter in Guangzhou, China, *Sci Total Environ*, 633, 1571-1578,  
581 10.1016/j.scitotenv.2018.03.293, 2018.
- 582 Lorenzo, R. D., Place, B. K., Vandenboer, T. C., and Young, C. J.: Composition of Size-Resolved Aged Boreal  
583 Fire Aerosols: Brown Carbon, Biomass Burning Tracers, and Reduced Nitrogen, *ACS Earth and Space  
584 Chemistry*, 2, 278-285, 10.1021/acsearthspacechem.7b00137, 2018.
- 585 Ma, W. L., Li, Y. F., Qi, H., Sun, D. Z., Liu, L. Y., and Wang, D. G.: Seasonal variations of sources of polycyclic  
586 aromatic hydrocarbons (PAHs) to a northeastern urban city, China, *Chemosphere*, 79, 441-447,  
587 10.1016/j.chemosphere.2010.01.048, 2010.
- 588 Miyazaki, Y., Kondo, Y., Takegawa, N., Komazaki, Y., Fukuda, M., Kawamura, K., Mochida, M., Okuzawa, K.,



- 589 and Weber, R. J.: Time-resolved measurements of water-soluble organic carbon in Tokyo, *Journal of*  
590 *Geophysical Research Atmospheres*, 111, -, 10.1029/2006JD007125, 2006.
- 591 Moosmuller, H., Chakrabarty, R. K., and Arnott, W. P.: Aerosol light absorption and its measurement: A review, *J.*  
592 *Quant. Spectrosc. Radiat. Transf.*, 110, 844-878, 10.1016/j.jqsrt.2009.02.035, 2009.
- 593 Nakayama, T., Sato, K., Matsumi, Y., Imamura, T., Yamazaki, A., and Uchiyama, A.: Wavelength and NOx  
594 dependent complex refractive index of SOAs generated from the photooxidation of toluene, *Atmospheric*  
595 *Chemistry and Physics*, 13, 531-545, 10.5194/acp-13-531-2013, 2013.
- 596 Nguyen-Duy, D., and Chang, M. B.: Review on characteristics of PAHs in atmosphere, anthropogenic sources  
597 and control technologies, *Science of the Total Environment*, 609, 682-693, 10.1016/j.scitotenv.2017.07.204,  
598 2017.
- 599 Pavuluri, C. M., Kawamura, K., and Swaminathan, T.: Time-resolved distributions of bulk parameters, diacids,  
600 ketoacids and  $\alpha$ -dicarbonyls and stable carbon and nitrogen isotope ratios of TC and TN in tropical Indian  
601 aerosols: Influence of land/sea breeze and secondary processes, *Atmospheric Research*, 153, 188-199,  
602 10.1016/j.atmosres.2014.08.011, 2015.
- 603 Peng, J., Hu, M., Guo, S., Du, Z., Zheng, J., Shang, D., Zamora, M. L., Zeng, L., Shao, M., Wu, Y.-S., Zheng, J.,  
604 Wang, Y., Glen, C. R., Collins, D. R., Molina, M. J., and Zhang, R.: Markedly enhanced absorption and  
605 direct radiative forcing of black carbon under polluted urban environments, *Proceedings of the National*  
606 *Academy of Sciences of the United States of America*, 113, 4266-4271, 10.1073/pnas.1602310113, 2016.
- 607 Ping, X., Zhou, X., Duan, J., Tan, J., He, K., Yuan, C., Ma, Y., and Zhang, Y.: Chemical characteristics of  
608 water-soluble organic compounds (WSOC) in PM 2.5 in Beijing, China: 2011–2012, *Atmospheric Research*,  
609 183, 104-112, 10.1016/j.atmosres.2016.08.020, 2017.
- 610 Qian, Y., Yasunari, T. J., Doherty, S. J., Flanner, M. G., Lau, W. K. M., Ming, J., Wang, H., Wang, M., Warren, S.  
611 G., and Zhang, R.: Light-absorbing particles in snow and ice: Measurement and modeling of climatic and  
612 hydrological impact, *Advances in Atmospheric Sciences*, 32, 64-91, 10.1007/s00376-014-0010-0, 2015.
- 613 Ren, Y., Wang, G., Wu, C., Wang, J., Li, J., Zhang, L., Han, Y., Liu, L., Cao, C., Cao, J., He, Q., and Liu, X.:  
614 Changes in concentration, composition and source contribution of atmospheric organic aerosols by shifting  
615 coal to natural gas in Urumqi, *Atmospheric Environment*, 148, 306-315, 10.1016/j.atmosenv.2016.10.053,  
616 2017.
- 617 Saleh, R., Hennigan, C. J., McMeeking, G. R., Chuang, W. K., Robinson, E. S., Coe, H., Donahue, N. M., and  
618 Robinson, A. L.: Absorptivity of brown carbon in fresh and photo-chemically aged biomass-burning  
619 emissions, *Atmospheric Chemistry and Physics*, 13, 7683-7693, 10.5194/acp-13-7683-2013, 2013.
- 620 Saleh, R., Robinson, E. S., Tkacik, D. S., Ahern, A. T., Liu, S., Aiken, A. C., Sullivan, R. C., Presto, A. A., Dubey,  
621 M. K., Yokelson, R. J., Donahue, N. M., and Robinson, A. L.: Brownness of organics in aerosols from  
622 biomass burning linked to their black carbon content, *Nature Geoscience*, 7, 647-650, 10.1038/ngeo2220,  
623 2014.
- 624 Satish, R. V., Shamjad, P. M., Thamban, N. M., Tripathi, S. N., and Rastogi, N.: Temporal Characteristics of  
625 Brown Carbon over the Central Indo-Gangetic Plain, *Environmental Science & Technology*, 51, 6765-6772,  
626 10.1021/acs.est.7b00734, 2017.
- 627 Shamjad, P. M., Satish, R. V., Thamban, N. M., Rastogi, N., and Tripathi, S. N.: Absorbing Refractive Index and  
628 Direct Radiative Forcing of Atmospheric Brown Carbon over Gangetic Plain, *ACS EARTH AND SPACE*  
629 *CHEMISTRY*, 2, 31-37, 10.1021/acsearthspacechem.7b00074, 2017.
- 630 Shen, Z., Zhang, Q., Cao, J., Zhang, L., Lei, Y., Huang, Y., Huang, R. J., Gao, J., Zhao, Z., Zhu, C., Yin, X.,  
631 Zheng, C., Xu, H., and Liu, S.: Optical properties and possible sources of brown carbon in PM 2.5 over





- 632 Xi'an, China, *Atmospheric Environment*, 150, 322-330, 10.1016/j.atmosenv.2016.11.024, 2017.
- 633 Smith, J. D., Sio, V., Yu, L., Zhang, Q., and Anastasio, C.: Secondary organic aerosol production from aqueous  
634 reactions of atmospheric phenols with an organic triplet excited state, *Environmental Science & Technology*,  
635 48, 1049-1057 10.1021/es4045715, 2014.
- 636 Sumlin, B. J., Pandey, A., Walker, M. J., Pattison, R. S., Williams, B. J., and Chakrabarty, R. K.: Atmospheric  
637 Photooxidation Diminishes Light Absorption by Primary Brown Carbon Aerosol from Biomass Burning,  
638 *Environmental Science & Technology Letters*, 4, 540-545, 10.1021/acs.estlett.7b00393, 2017.
- 639 Sun, J., Zhi, G., Hitzenberger, R., Chen, Y., Tian, C., Zhang, Y., Feng, Y., Cheng, M., Zhang, Y., and Cai, J.:  
640 Emission factors and light absorption properties of brown carbon from household coal combustion in China,  
641 *Atmospheric Chemistry and Physics*, 17, 4769-4780, 10.5194/acp-17-4769-2017, 2017.
- 642 Teich, M., Van Pinxteren, D., Wang, M., Kecorius, S., Wang, Z., Müller, T., Močnik, G., and Herrmann, H.:  
643 Contributions of nitrated aromatic compounds to the light absorption of water-soluble and particulate brown  
644 carbon in different atmospheric environments, *Atmospheric Chemistry and Physics*, 17, 1-24,  
645 10.5194/acp-17-1653-2017, 2017.
- 646 Wang, D., Tian, F., Yang, M., Liu, C., and Li, Y. F.: Application of positive matrix factorization to identify  
647 potential sources of PAHs in soil of Dalian, China, *Environmental Pollution*, 157, 1559-1564,  
648 10.1016/j.envpol.2009.01.003, 2009a.
- 649 Wang, G., Kawamura, K., Xie, M., and Hu, S.: Size-distributions of n-hydrocarbons, PAHs and hopanes and their  
650 sources in the urban, mountain and marine atmospheres over East Asia, *Atmospheric Chemistry & Physics*,  
651 9, 8869-8882, 10.5194/acp-9-8869-2009, 2009b.
- 652 Wang, G., Xie, M., Hu, S., Gao, S., Tachibana, E., and Kawamura, K.: Dicarboxylic acids, metals and isotopic  
653 compositions of C and N in atmospheric aerosols from inland China: implications for dust and coal burning  
654 emission and secondary aerosol formation, *Atmospheric Chemistry and Physics*, 10, 6087-6096,  
655 10.5194/acp-10-6087-2010, 2010.
- 656 Wang, G., Zhang, R., Gomez, M. E., Yang, L., Zamora, M. L., Hu, M., Lin, Y., Peng, J., Guo, S., Meng, J., Li, J.,  
657 Cheng, C., Hu, T., Ren, Y., Wang, Y., Gao, J., Cao, J., An, Z., Zhou, W., Li, G., Wang, J., Tian, P.,  
658 Marrero-Ortiz, W., Secret, J., Du, Z., Zheng, J., Shang, D., Zeng, L., Shao, M., Wang, W., Huang, Y., Wang,  
659 Y., Zhu, Y., Li, Y., Hu, J., Pan, B., Cai, L., Cheng, Y., Ji, Y., Zhang, F., Rosenfeld, D., Liss, P. S., Duce, R. A.,  
660 Kolb, C. E., and Molina, M. J.: Persistent sulfate formation from London Fog to Chinese haze, *Proceedings  
661 of the National Academy of Sciences of the United States of America*, 113, 13630-13635,  
662 10.1073/pnas.1616540113, 2016.
- 663 Wang, G. H., Zhou, B. H., Cheng, C. L., Cao, J. J., Li, J. J., Meng, J. J., Tao, J., Zhang, R. J., and Fu, P. Q.:  
664 Impact of Gobi desert dust on aerosol chemistry of Xi'an, inland China during spring 2009: differences in  
665 composition and size distribution between the urban ground surface and the mountain atmosphere,  
666 *Atmospheric Chemistry and Physics*, 13, 819-835, 10.5194/acp-13-819-2013, 2013.
- 667 Wang, J., Ho, S. S. H., Cao, J., Huang, R., Zhou, J., Zhao, Y., Xu, H., Liu, S., Wang, G., and Shen, Z.:  
668 Characteristics and major sources of carbonaceous aerosols in PM 2.5 from Sanya, China, *Science of the  
669 Total Environment*, 530-531, 110-119, 10.1016/j.scitotenv.2015.05.005, 2015.
- 670 Wang, J., Cao, J., Dong, Z., Guinot, B., Gao, M., Huang, R., Han, Y., Huang, Y., Ho, S., and Shen, Z.: Seasonal  
671 variation, spatial distribution and source apportionment for polycyclic aromatic hydrocarbons (PAHs) at  
672 nineteen communities in Xi'an, China: The effects of suburban scattered emissions in winter, *Environmental  
673 Pollution*, 1330-1343, 10.1016/j.envpol.2017.08.106, 2017.
- 674 Wang, X., Heald, C. L., Ridley, D. A., Schwarz, J. P., Spackman, J. R., Perring, A. E., Coe, H., Liu, D., and



- 675 Clarke, A. D.: Exploiting simultaneous observational constraints on mass and absorption to estimate the  
676 global direct radiative forcing of black carbon and brown carbon, *Atmospheric Chemistry and Physics*, 14,  
677 17527-17583, 10.5194/acp-14-10989-2014, 2014.
- 678 Washenfelder, R. A., Attwood, A. R., Brock, C. A., Guo, H., Xu, L., Weber, R. J., Ng, N. L., Allen, H. M., Ayres,  
679 B. R., Baumann, K., Cohen, R. C., Draper, D. C., Duffey, K. C., Edgerton, E., Fry, J. L., Hu, W. W.,  
680 Jimenez, J. L., Palm, B. B., Romer, P., Stone, E. A., Wooldridge, P. J., and Brown, S. S.: Biomass burning  
681 dominates brown carbon absorption in the rural southeastern United States, *Geophysical Research Letters*,  
682 42, 653-664, 10.1002/2014gl062444, 2015.
- 683 Wu, C., Wang, G., Wang, J., Li, J., Ren, Y., Zhang, L., Cao, C., Li, J., Ge, S., and Xie, Y.: Chemical  
684 characteristics of haze particles in Xi'an during Chinese Spring Festival: Impact of fireworks burning,  
685 *Journal of Environmental Sciences*, 179-187, 10.1016/j.jes.2018.04.008, 2018.
- 686 Wu, C., Wang, G., Cao, C., Li, J., Li, J., Wu, F., Huang, R., Cao, J., Han, Y., Ge, S., Xie, Y., Xue, G., and Wang,  
687 X.: Chemical characteristics of airborne particles in Xi'an, inland China during dust storm episodes:  
688 Implications for heterogeneous formation of ammonium nitrate and enhancement of N-deposition,  
689 *Environmental Pollution*, 244, 877-884, 10.1016/j.envpol.2018.10.019, 2019.
- 690 Xie, M., Chen, X., Hays, M. D., Lewandowski, M., Offenberg, J., Kleindienst, T. E., and Holder, A. L.: Light  
691 Absorption of Secondary Organic Aerosol: Composition and Contribution of Nitroaromatic Compounds,  
692 *Environmental Science & Technology*, 51, 11607-11616, 10.1021/acs.est.7b03263, 2017.
- 693 Xie, M., Shen, G., Holder, A. L., Hays, M. D., and Jetter, J. J.: Light absorption of organic carbon emitted from  
694 burning wood, charcoal, and kerosene in household cookstoves, *Environmental Pollution*, 240, 60-67,  
695 10.1016/j.envpol.2018.04.085, 2018.
- 696 Yan, C., Zheng, M., Sullivan, A. P., Bosch, C., Desyaterik, Y., Andersson, A., Li, X., Guo, X., Zhou, T., and  
697 Örjan, G.: Chemical characteristics and light-absorbing property of water-soluble organic carbon in Beijing:  
698 Biomass burning contributions, *Atmospheric Environment*, 121, 4-12, 10.1016/j.atmosenv.2015.05.005,  
699 2015.
- 700 Yan, C., Zheng, M., Bosch, C., Andersson, A., Desyaterik, Y., Sullivan, A. P., Collett, J. L., Zhao, B., Wang, S.,  
701 He, K., and Gustafsson, O.: Important fossil source contribution to brown carbon in Beijing during winter,  
702 *Scientific Reports*, 7, 43182, 10.1038/srep43182, 2017.
- 703 Yan, J., Wang, X., Gong, P., Wang, C., and Cong, Z.: Review of brown carbon aerosols: Recent progress and  
704 perspectives, *Science of The Total Environment*, 634, 1475-1485, 10.1016/j.scitotenv.2018.04.083, 2018.
- 705 Yang, H., Xu, J., Wu, W. S., Wan, C. H., and Yu, J. Z.: Chemical Characterization of Water-Soluble Organic  
706 Aerosols at Jeju Island Collected During ACE-Asia, *Environmental Chemistry*, 1, 13-17, 10.1071/EN04006,  
707 2004.
- 708 Zhai, J., Lu, X., Li, L., Zhang, Q., Zhang, C., Chen, H., Yang, X., and Chen, J.: Size-resolved chemical  
709 composition, effective density, and optical properties of biomass burning particles, *Atmospheric Chemistry  
710 and Physics*, 17, 1-25, 10.5194/acp-17-7481-2017, 2017.
- 711 Zhang, X., Hecobian, A., Zheng, M., Frank, N. H., and Weber, R. J.: Biomass burning impact on PM<sub>2.5</sub> over the  
712 southeastern US during 2007: integrating chemically speciated FRM filter measurements, MODIS fire  
713 counts and PMF analysis, *Atmospheric Chemistry and Physics*, 10, 6839-6853, 10.5194/acp-10-6839-2010,  
714 2010.
- 715 Zhang, X., Lin, Y. H., Surratt, J. D., Zotter, P., Prévôt, A. S. H., and Weber, R. J.: Light-absorbing soluble organic  
716 aerosol in Los Angeles and Atlanta: A contrast in secondary organic aerosol, *Geophysical Research Letters*,  
717 38, 759-775, 10.1029/2011GL049385, 2011.



- 718 Zhang, Z., Gao, J., Engling, G., Tao, J., Chai, F., Zhang, L., Zhang, R., Sang, X., Chan, C. Y., and Lin, Z.:  
719 Characteristics and applications of size-segregated biomass burning tracers in China's Pearl River Delta  
720 region, *Atmospheric Environment*, 102, 290-301, 10.1016/j.atmosenv.2014.12.009, 2015.  
721 Zhao, M., Huang, Z., Qiao, T., Zhang, Y., Xiu, G., and Yu, J.: Chemical characterization, the transport pathways  
722 and potential sources of PM<sub>2.5</sub> in Shanghai: Seasonal variations, *Atmospheric Research*, 158-159, 66-78,  
723 10.1016/j.atmosres.2015.02.003, 2015a.  
724 Zhao, R., Lee, A. K. Y., Huang, L., Li, X., Yang, F., and Abbatt, J. P. D.: Photochemical processing of aqueous  
725 atmospheric brown carbon, *Atmospheric Chemistry and Physics*, 15, 6087-6100,  
726 10.5194/acp-15-6087-2015, 2015b.  
727 Zong, Z., Wang, X., Tian, C., Chen, Y., Qu, L., Ji, L., Zhi, G., Li, J., and Zhang, G.: Source apportionment of  
728 PM<sub>2.5</sub> at a regional background site in North China using PMF linked with radiocarbon analysis: insight  
729 into the contribution of biomass burning, *Atmospheric Chemistry and Physics*, 16, 11249-11265,  
730 10.5194/acp-16-11249-2016, 2016.

731

732

### 733 **Table List**

734 Table 1. Concentrations of organic carbon in PM<sub>2.5</sub> and meteorological conditions during  
735 winter and summer of 2017 in Xi'an, inland China.

736

737 Table 2. Comparison on light absorption ( $abs_{\lambda=365nm}$ ), MAC, and AAE values of water-extracts of  
738 PM<sub>2.5</sub> in Xi'an, China with those in other cities.

739

740 Table 3. Complex refractive index ( $k$ ) of brown carbon from samples extracted by water in  
741 two seasons.

742

743

### 744 **Figure caption**

745 Fig. 1 Temporal variations of WSOC, OC, PM<sub>2.5</sub>, and  $abs_{\lambda=365nm}$  of PM<sub>2.5</sub> samples extracted by  
746 water (H<sub>2</sub>O extraction) and methanol (MeOH extraction) during winter (**a** and **c**) and summer  
747 (**b** and **d**).

748

749 Fig. 2 Seasonal average values of  $abs_{\lambda=365nm}$ , AAE, and MAC extracted by MeOH and H<sub>2</sub>O.  
750 AAE is calculated by linear regression fit  $\log(abs_{\lambda=365nm})$  versus  $\log(\lambda)$  in the wavelength  
751 range of 300–450 nm. (The shadows indicating the standard deviations)

752

753 Fig. 3 Size distributions of  $abs_{\lambda=365nm}$  and MAC of PM<sub>2.5</sub> samples extracted by water during  
754 the winter and summer of 2017 in Xi'an.

755

756 Fig. 4 Comparison of  $abs_{\lambda=365nm}$  of samples between predicted by Mie theory and extracted by



757 water for different particle size ( $D_p < 2.1\mu\text{m}$ ).

758

759 Fig. 4 Comparison of  $\text{abs}_{\lambda=365\text{nm}}$  of samples predicted by Mie theory with those of samples  
760 extracted by water for different particle sizes ( $D_p < 2.1\mu\text{m}$ ).

761

762 Fig. 5 Temporal variations of  $\text{PM}_{2.5}$ , meteorological parameters,  $\text{abs}_{\lambda=365\text{nm}}$  of carbonaceous  
763 matter and organic compounds in the period of January 10<sup>th</sup> -20<sup>th</sup> (The cyan shadow indicates  
764 a haze period from January 12<sup>th</sup> to 19<sup>th</sup> with a daily  $\text{PM}_{2.5} > 75\mu\text{g}/\text{m}^3$ ).

765

766 Fig.6 Linear fit regressions for the ratio of light absorption of methanol-extracts to light  
767 absorption of EC ( $\text{abs}_{\lambda=365\text{nm}}\text{-MeOH}/\text{abs}_{\lambda=550\text{nm}}\text{-EC}$ ) with (a and b)  $\delta^{13}\text{C}$  and (c and d) relative  
768 abundance of nitrophenol to EC (Nitrophenol/EC) in the day- and night- $\text{PM}_{2.5}$  samples  
769 collected during the haze period of January 12<sup>th</sup> to 19<sup>th</sup> (corresponding to the cyan shadow in  
770 Figure 5) in Xi'an.

771

772 Fig. 7 Factor profiles resolved by PMF mode during the winter and summer sampling period.  
773 The bars represent the concentrations of species and the dots represent the contributions of  
774 species appointed to the factors (the summer and winter samples were merged together for the  
775 PMF analysis due to the limited number of samples).

776

777 Fig. 8 Source apportionment for airborne fine particulate BrC in Xi'an during the campaign.

778

779

780

781

782

783 Table 1. Concentrations of organic carbon in  $\text{PM}_{2.5}$  and meteorological conditions during  
784 winter and summer of 2017 in Xi'an, inland China.

	Winter	Summer
I. Mass concentrations of organic matter in $\text{PM}_{2.5}$		
WSOC ( $\mu\text{g}/\text{m}^3$ )	$23 \pm 13$	$5.8 \pm 1.4$
OC ( $\mu\text{g}/\text{m}^3$ )	$41 \pm 25$	$8.4 \pm 2.4$
PAHs ( $\text{ng}/\text{m}^3$ )	$149 \pm 89$	$8.1 \pm 6.5$
OPAHs ( $\text{ng}/\text{m}^3$ )	$174 \pm 98$	$17 \pm 8.7$
Nitrophenols ( $\text{ng}/\text{m}^3$ )	$17 \pm 12$	$0.40 \pm 0.27$
Levoglucosan ( $\text{ng}/\text{m}^3$ )	$739 \pm 432$	$29 \pm 22$
II. $\text{PM}_{2.5}$ and meteorological parameters		
$\text{PM}_{2.5}$ ( $\mu\text{g}/\text{m}^3$ )	$194 \pm 141$	$37 \pm 16$
T ( $^{\circ}\text{C}$ )	$2.6 \pm 2.9$	$31 \pm 5.4$
RH (%)	$60 \pm 20$	$58 \pm 19$
Visibility (km)	$7.0 \pm 7.0$	$21 \pm 11$

785

786



787 Table 2. Comparison on light absorption ( $abs_{\lambda=365nm}$ ), MAC, and AAE values of water-extracts of  
 788  $PM_{2.5}$  in Xi'an, China with those in other cities.

Location	Time	$abs_{\lambda=365nm}$ (M/m)		MAC ( $m^2/g$ )		AAE		References
		Winter	Summer	Winter	Summer	Winter	Summer	
Xi'an, China	2016-2017	49±32 <sup>a</sup>	5.2±2.1 <sup>a</sup>	1.3±0.03 <sup>a</sup>	0.8 <sup>a</sup> ±0.1 <sup>a</sup>	6.1±9.7 <sup>a</sup>	5.5±8.8 <sup>a</sup>	This study
		28±16	3.5±1.7	1.2±0.06	1.1±0.2	5.3±8.5	4.8±7.7	
	2008-2009	46±20 <sup>a</sup>	8.3±2.3 <sup>a</sup>	1.3 <sup>a</sup>	0.7 <sup>a</sup>	6.0 <sup>a</sup>	6.0 <sup>a</sup>	Huang et al. (2018)
		25±12	5.0±1.3	1.7	1.0	5.7	5.7	
Beijing, China	2010-2011	10±8.6	3.7±3.8	1.3	0.5			Du et al. (2014)
	2011	10±6.9		1.2		7.3		Cheng et al. (2016)
Nanjing, China	2013	14±5.2	4.6±2.2	1.5	0.7	5.3	5.8	Yan et al. (2015)
	2015-2016	9.4 ± 4.7	3.3±2.4	1.0	0.5	6.7	7.3	Chen et al. (2018)
Guangzhou, China	2012	3.6±1.3		0.8		5.3		Liu et al. (2018)
Delhi, India	2010-2011			1.6		5.1		Kirillova et al. (2014)
	2015-2016	24±19		1.2				Satish et al. (2017)
Indo- Gangetic Plain India	2011	40 ± 18 <sup>b</sup>		1.3 <sup>b</sup>		5.1 <sup>b</sup>		Bachi et al. (2016)
		52 ± 27 <sup>c</sup>		1.3 <sup>c</sup>		5.3 <sup>c</sup>		
Seoul, Korea	2013-2013	11 <sup>a</sup>	5.8 <sup>a</sup>	0.9 <sup>a</sup>	1.5 <sup>a</sup>	5.5 <sup>a</sup>	4.1 <sup>a</sup>	Kim et al.(2016)
		7.3	0.9	1.0	0.3	5.8	8.7	
Atlanta, US	2010		0.6±0.4		1.2-0.2		3.4	Zhang et al. (2011)
Los Angeles Basin, US	2010		0.4-1.6		0.7		7.6	Zhang et al. (2013)

789 Notes: <sup>a</sup> solution extracted by MeOH; <sup>b</sup> samples collected at day time; <sup>c</sup> samples collected in the night

790

791

792

793

794

795

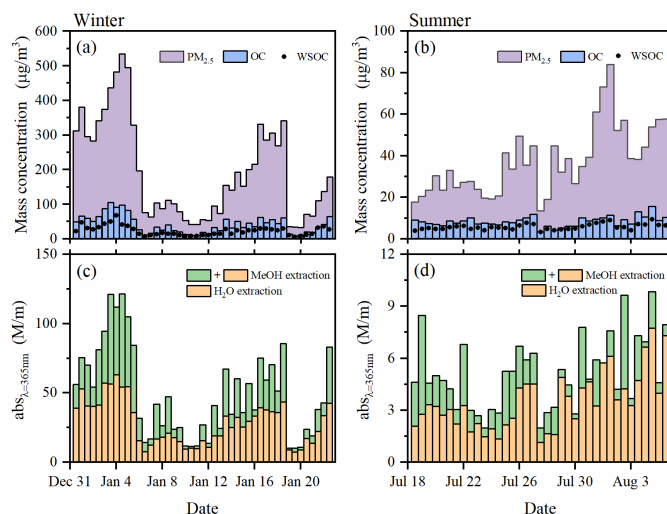
796 Table 3. Complex refractive index ( $k$ ) of brown carbon from samples extracted by water in  
 797 two seasons.

Particle size ( $\mu m$ )	Winter	Summer
1.31	0.047 ± 0.005	0.021 ± 0.010
0.73	0.048 ± 0.008	0.033 ± 0.010
0.45	0.048 ± 0.013	0.031 ± 0.009
0.18	0.038 ± 0.016	0.026 ± 0.008

798

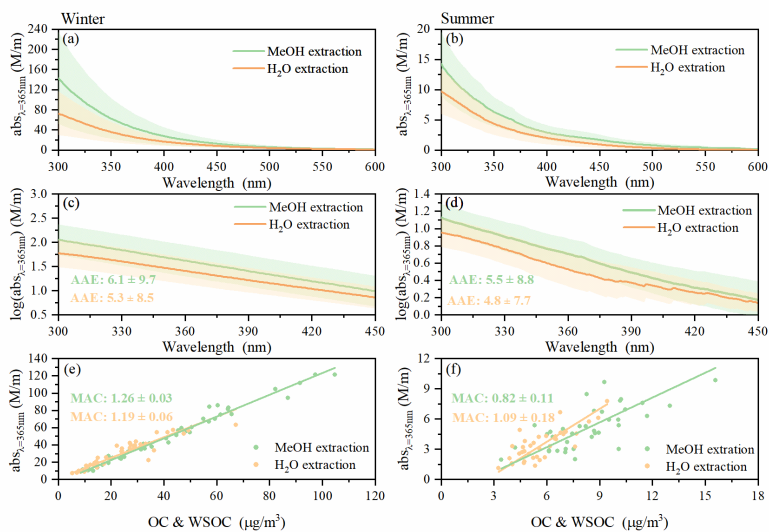
799

800



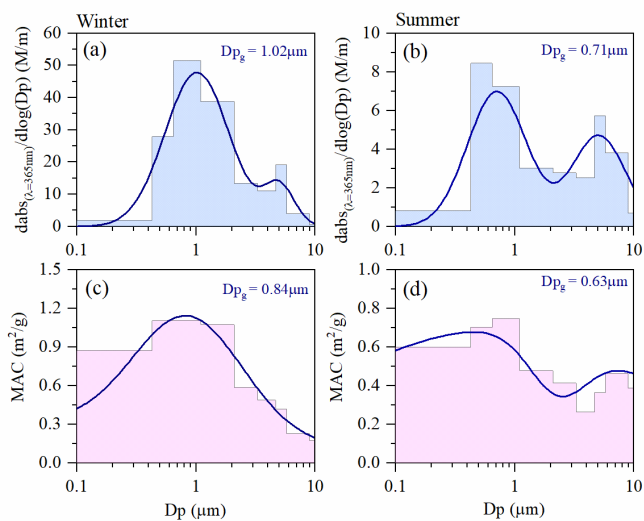
801  
 802  
 803  
 804  
 805  
 806

Fig. 1 Temporal variations of WSOC, OC, PM<sub>2.5</sub>, and  $\text{abs}_{\lambda=365\text{nm}}$  of PM<sub>2.5</sub> samples extracted by water (H<sub>2</sub>O-extraction) and methanol (MeOH-extraction) during winter (a and c) and summer (b and d).



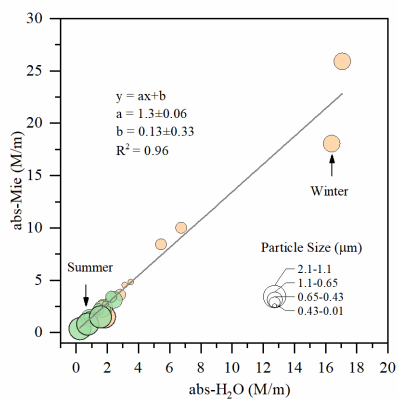
807  
 808  
 809  
 810  
 811  
 812

Fig. 2 Seasonal average values of  $\text{abs}_{\lambda=365\text{nm}}$ , AAE, and MAC extracted by MeOH and H<sub>2</sub>O. AAE is calculated by linear regression fit  $\log(\text{abs}_{\lambda=365\text{nm}})$  versus  $\log(\lambda)$  in the wavelength range of 300–450 nm. (The shadows indicating the standard deviations)



813  
814  
815  
816  
817  
818

Fig. 3 Size distributions of  $\text{abs}_{\lambda=365\text{nm}}$  and MAC of  $\text{PM}_{2.5}$  samples extracted by water during the winter and summer of 2017 in Xi'an.

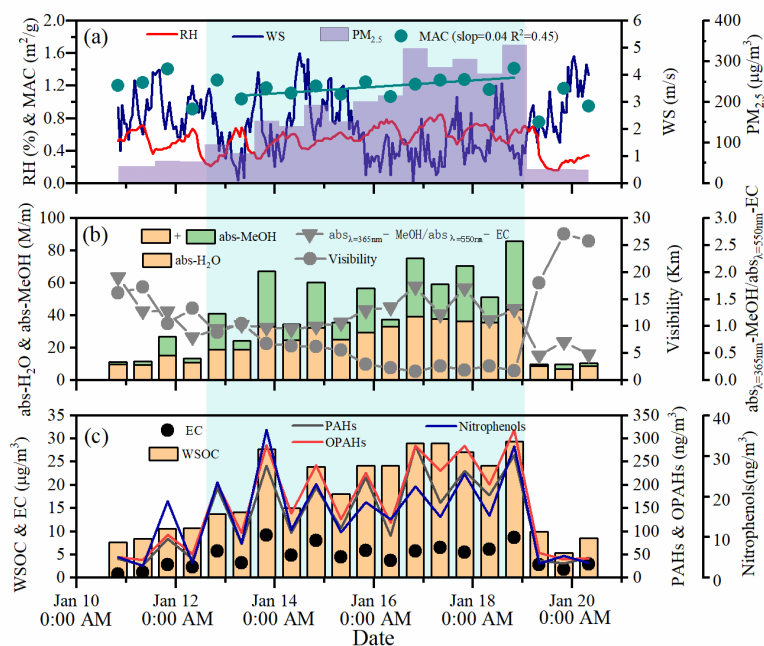


819  
820  
821  
822  
823  
824  
825  
826  
827  
828

Fig. 4 Comparison of  $\text{abs}_{\lambda=365\text{nm}}$  of samples predicted by Mie theory with those of samples extracted by water for different particle sizes ( $D_p < 2.1\mu\text{m}$ ).



829  
 830  
 831  
 832  
 833



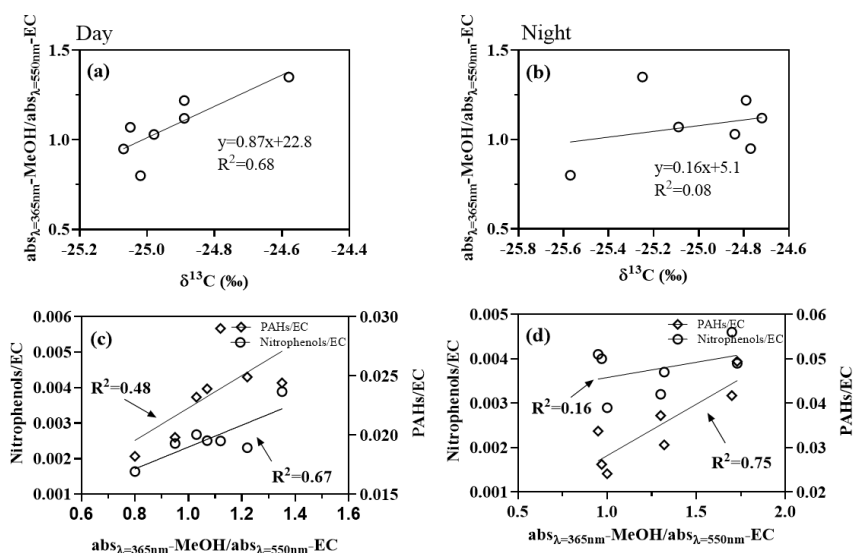
834  
 835 Fig. 5 Temporal variations of  $PM_{2.5}$ , meteorological parameters,  $abs_{\lambda=365nm}$  of carbonaceous  
 836 matter and organic compounds in the period of January 10<sup>th</sup> -20<sup>th</sup> (The cyan shadow indicates  
 837 a haze period from January 12<sup>th</sup> to 19<sup>th</sup> with a daily  $PM_{2.5} > 75 \mu g/m^3$ ).

838  
 839  
 840  
 841  
 842  
 843  
 844  
 845  
 846  
 847  
 848  
 849  
 850  
 851



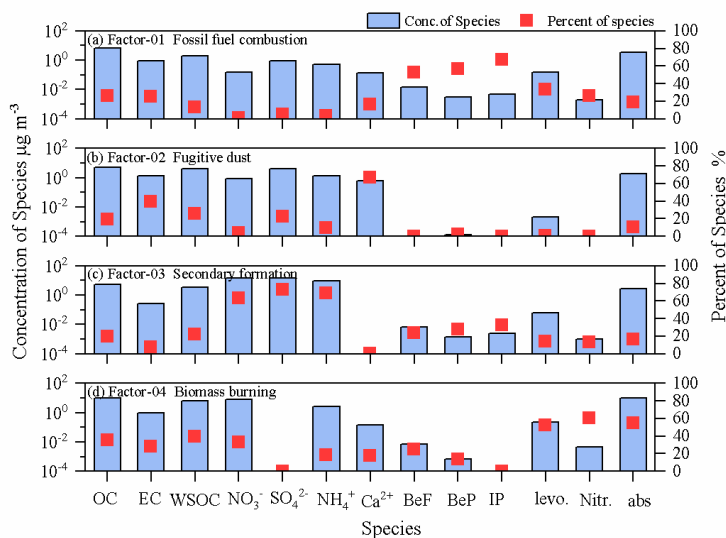


852  
853  
854  
855  
856  
857



858  
859 Fig.6 Linear fit regressions for the ratio of light absorption of methanol-extracts to light  
860 absorption of EC ( $\text{abs}_{\lambda=365\text{nm}}\text{-MeOH}/\text{abs}_{\lambda=550\text{nm}}\text{-EC}$ ) with (a and b)  $\delta^{13}\text{C}$  and (c and d) relative  
861 abundance of nitrophenol to EC (Nitrophenols/EC) in the day- and night- $\text{PM}_{2.5}$  samples  
862 collected during the haze period of January 12<sup>th</sup> to 19<sup>th</sup> (corresponding to the cyan shadow in  
863 Figure 5) in Xi'an.

864  
865  
866  
867  
868  
869  
870  
871  
872



873

874 Fig. 7 Factor profiles resolved by PMF mode during the winter and summer sampling period.  
 875 The bars represent the concentrations of species and the dots represent the contributions of  
 876 species appointed to the factors (the summer and winter samples were merged together for the  
 877 PMF analysis due to the limited number of samples).

878

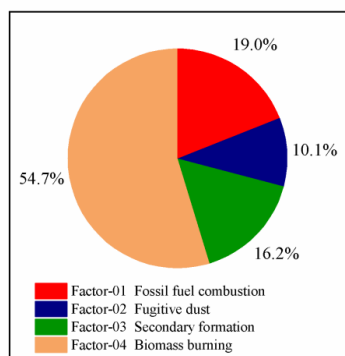
879

880

881

882

883



884

885 Fig. 8 Source apportionment for airborne fine particulate BrC in Xi'an during the campaign.